Delft University of Technology

CFD II: Discretization Techniques

AE4136

Lid Driven Cavity Problem

Authors:

Aaron Sequeira (5258766)

Aniruddha Paranjape (5285143)

June 13, 2022

Contents

List of Figures

Chapter 1

Introduction

This assignment deals with writing a solver for the Navier-Stokes equations for a lid driven cavity problem. The solver is based on the use of incidence and Hodge matrices. We also intend to solve the equations on a unit square. The domain is discretized into N $\times$ N grid, also known as the primal mesh, which contains information about the velocity fluxes. Associated with this primal mesh we have a dual grid which contains unknowns related to the pressure.

The Navier-Stokes equations on a unit square are given as:
Conservation of mass:

$$\nabla \cdot \vec{u} = 0 \tag{1.1}$$

Conservation of momentum:

$$\frac{\partial \vec{u}}{\partial t} + (u, \vec{\nabla})\vec{u} + \vec{\nabla} p = \frac{1}{\mathrm{Re}} \Delta \vec{u} \tag{1.2}$$

Where $\vec{u}$ is the velocity field and Re is the Reynolds number, which is a non dimensional value that relates the inertial forces to the viscous forces. This is given as:

$$\mathrm{Re} = \frac{\rho U L}{\mu} \tag{1.3}$$

Where ρ is the fluid density, μ is the fluid viscosity, U is the velocity, while L is the characteristic length scale.

As mentioned above, the unknowns lie on the primal and dual grids. In order to obtain these unknowns, the vector operations of the curl, divergence, and gradient are given by the incidence matrices, while switching from the primal to the dual grid is done through a Hodge matrix. A partially implicit time scheme is then used to then compute the unknown pressures and velocities from the final matrix system.

Chapter 2

Fundamental Concepts

2.1 Navier-Stokes Equations

We define the Navier-Stokes equation in the previous section. In this particular case we deal with incompressible flow with constant density. In particular we will try to understand the meaning of the terms.

2.1.1 Convective Term

In the momentum equation the convective term is represented by:

$$(u, \vec{\nabla})\vec{u} \tag{2.1}$$

This is non-linear term that models the momentum transport through the flow with the local velocity. The velocity field inside the brackets is the convective velocity, while the other velocity field is the momentum that is being convected by the convective velocity. We can use some identities to re-write the convective term as:

$$(u, \vec{\nabla})\vec{u} = \nabla\left(\frac{1}{2}||\vec{u}||^2\right) - \vec{u} \times (\nabla \times \vec{u}) \tag{2.2}$$

From this identity we abbreviate:

$$\vec{\xi} = \nabla \times \vec{u} \tag{2.3}$$

Where ξ represents the vorticity. From this, we get:

$$(u, \vec{\nabla})\vec{u} = \vec{\xi} \times \vec{u} + \nabla\left(\frac{1}{2}||\vec{u}||^2\right) \tag{2.4}$$

2.1.2 Diffusive Term

The term $\Delta\vec{u}$ is the diffusive term and is a result of the viscous contribution of flow. For incompressible flows, we can say that:

$$\Delta\vec{u} = -\vec{\nabla} \times \vec{\xi} \tag{2.5}$$

Plugging in the these equations back into the momentum equation, we can re-write the equation as:

$$\frac{\partial\vec{u}}{\partial t} - \vec{u} \times \vec{\xi} + \nabla P = -\frac{1}{\mathrm{Re}}\nabla \times \vec{xi} \tag{2.6}$$

where;

$$P = p + \frac{1}{2}||\vec{u}||^2 \tag{2.7}$$

2.1.3 Final System

From the above math, we can write the final system as:

$$\begin{aligned} \nabla \cdot \vec{u} &= 0 \\ \xi &= \nabla \times \vec{u} \\ \frac{\partial\vec{u}}{\partial t} - \vec{u} \times \vec{\xi} + \nabla P + \frac{1}{Re}\nabla \times \vec{\xi} &= 0 \end{aligned} \tag{2.8}$$

2.2 Incidence and Hodge Matrices

As mentioned before, Incidence and Hodge Matrices are used to represent the vector operations and to move from the primal mesh to the dual mesh. We take a closer look at them in this section.

2.2.1 Incidence Matrices

Specifically, incidence matrices are used to represent the vector operations:

$$\mathrm{div} \equiv \nabla \cdot \qquad \mathrm{curl} \equiv \nabla \times \qquad \mathrm{grad} \equiv \nabla \tag{2.9}$$

This of course means that the incidence matrices are an exact representative of a derivative. Conventionally, the concept of the derivative is defined on the mesh as:

$$f'(x_0) = \lim_{h \to 0} \frac{f(x_0 + h) - f(x_0)}{h} \tag{2.10}$$

In order to simulate the limit we have to go finer and finer grids such that we finally end up with the exact values. This however is not feasible as we end up with poor approximations. Instead we can define the derivatives through the boundary of geometric objects.

Depending on how the sense of the flux is defined through the boundaries, a value of 1,0, or -1 is applied and a matrix is then generated by associating for example the surface to the edges or the edges to points. For this assignment, we have a two-dimensional problem which means we define two incidence matrices, namely:

- $\mathbb{E}^{1,0}$: Associates the edges to points and represents the curl operation
- $\mathbb{E}^{2,1}$: Associates the surfaces to the edges and represents the divergence operation

A matrix takes the shape:

$$\mathbb{E}^{1,0} = \begin{bmatrix} 1 & 0 & \dots \\ \vdots & \ddots & \\ 1 & & -1 \end{bmatrix}$$

2.2.2 Hodge Matrices

The Hodge matrices are used to relate quantities between the primal and dual meshes. The Hodge matrices are always in the form of diagonal matrices. For example, the degrees of freedom relation between the flux and the circulation are given as:

$$\begin{aligned} u_{flux} &= \int_e u \mathrm{d}y \\ u_{circ} &= \int_{\bar{e}} u \mathrm{d}x \end{aligned} \tag{2.11}$$

Assuming that the flux and circulation velocities are constant along an edge, we get:

$$\begin{aligned} u_{flux} &= \int_e u \mathrm{d}y \approx u \int_e \mathrm{d}y = u|e| \\ u_{circ} &= \int_{\bar{e}} u \mathrm{d}x \approx u \int_{\bar{e}} \mathrm{d}x = u|\bar{e}| \end{aligned} \tag{2.12}$$

Thus, the relation between the two quantities is given as:

$$u_{flux} = \frac{|e|}{|\bar{e}|} u_{circ} \tag{2.13}$$

In a similar fashion the circulation we can develop a relationship between the vorticity on the dual grid to the vorticity on the primal grid.

For this assignment we use the following Hodge matrices:

- $\mathbb{H}^{\tilde{1},0}$: Relates the velocity of the flux on the primal edge to the circulation along the dual edge, provided that the velocities are constant along the edges
- $\mathbb{H}^{\tilde{0},2}$: Relates the vorticity on the surface of a dual grid to the vorticity at the primal points, provided that the vorticity at the primal points is assumed to be constant

A matrix takes the shape:

$$\mathbb{E}^{1,0} = \begin{bmatrix} 1 & 0 & \dots \\ \vdots & \ddots & \\ 0 & & 1 \end{bmatrix}$$

2.2.3 De Rahm Sequence

The De Rahm sequences gives an overarching picture of the results of the vector operations as we apply the gradient, curl, or divergence. When there is the element of the dual mesh, we extent this De Rahm sequence to a double De Rahm sequence. In this sequence, we can do the derivatives along the horizontal arrows. This is done on the primal and the dual meshes. The two are then connected by the Hodge matrices which allow us to go from one to other.

Physically, the vertical relations (Hodge matrices) model the constitutive models, while the horizontal relations model the conservation laws, definitions and equilibrium conditions.

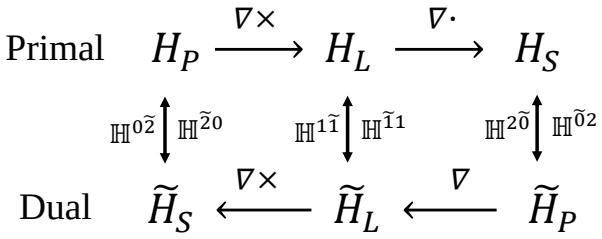

Figure 2.1: Double De Rahm sequence between the primal and dual grids

Thus, the De Rahm sequence becomes a useful tool in understanding the flow of the assignment and when an operation must be performed to achieve the desired result.

2.3 Discrete System

Once the matrices are constructed, we can re-write the original Navier-Stokes equations in a discrete form. The discrete form contains the Hodge and Incidence matrices. All the variables are treated as being defined on the dual mesh, when we need to perform an operation on to the primal mesh, a Hodge matrix is used to perform the operation.

This final discrete system is represented as:

$$\begin{aligned} \tilde{\mathbb{E}}^{(2,1)} H^{\tilde{1},1} \vec{u}^{n+1} + \vec{u}_{\text{norm}} &= 0 \\ \xi^n = \mathbb{E}^{(2,1)} \vec{u}^n & \\ \frac{\vec{u}^{n+1} - \vec{u}^n}{\Delta t} + \text{ conv }^n + \mathbb{E}^{(1,0)} P^{n+1} + \frac{1}{Re} H^{1,1} \tilde{\mathbb{E}}^{(1,0)} H^{\tilde{0},2} \left(\xi^n + \xi_{\text{prescr}}\right) &= 0 \end{aligned} \tag{2.14}$$

Where n and $n+1$ represent the time level at which the variables are being evaluated. In order to ensure that the new velocity field at the next time step follows the conservation of mass, we have to add

$$\tilde{\mathbb{E}}^{(2,1)} H^{1,1}$$

to the momentum equation. We aim to eliminate the $\vec{u}^{n+1}$ term from the conservation of mass and momentum to end up with an equation of the pressure, this is done as follows:

$$\tilde{\mathbb{E}}^{(2,1)} H^{\tilde{1},1} \vec{u}^{n+1} + \vec{u}_{\text{norm}} = 0$$

Re-arranging:

$$\vec{u}^{n+1} = -(\tilde{\mathbb{E}}^{(2,1)} \mathbb{H}^{(\tilde{1},1)})^{-1} \vec{u}_{\text{norm}}$$

We can use the above result as a substitution into the momentum equation. But before we shall re-arrange the momentum equation to make the process easier:

$$\mathbb{E}^{(1,0)} P^{n+1} = -\left(\frac{\vec{u}^{n+1} - \vec{u}^n}{\Delta t}\right) - \text{ conv }^n - \frac{1}{Re} H^{1,1} \tilde{\mathbb{E}}^{(1,0)} H^{\tilde{0},2} \left(\xi^n + \xi_{\text{prescr}}\right)$$

Making the substitution:

$$\mathbb{E}^{(1,0)} P^{n+1} = -\frac{1}{\Delta t}\left((\tilde{\mathbb{E}}^{(2,1)} \mathbb{H}^{(\tilde{1},1)})^{-1} \vec{u}_{\text{norm}} - \vec{u}^n\right) - \text{ conv }^n - \frac{1}{Re} H^{1,1} \tilde{\mathbb{E}}^{(1,0)} H^{\tilde{0},2} \left(\xi^n + \xi_{\text{prescr}}\right)$$

Multiplying by $\tilde{\mathbb{E}}^{(2,1)} H^{\tilde{1},1}$, and -1 we get:

$$-\tilde{\mathbb{E}}^{(2,1)} H^{\tilde{1},1} \mathbb{E}^{(1,0)} P^{n+1} = \frac{\vec{u}_{\text{norm}}}{\Delta t} - \tilde{\mathbb{E}}^{(2,1)} H^{\tilde{1},1} \left(\frac{\vec{u}^n}{\Delta t} - \text{ conv }^n - \frac{1}{Re} H^{1,1} \tilde{\mathbb{E}}^{(1,0)} H^{\tilde{0},2} \left(\xi^n + \xi_{\text{prescr}}\right)\right)$$

As referenced in the assignment, we can write this in the form:

$$A\vec{P} = f$$

Where;

$$A = -\tilde{\mathbb{E}}^{(2,1)} H^{\tilde{1},1} \mathbb{E}^{(1,0)} \tag{2.15}$$

and

$$f = \tilde{\mathbb{E}}^{(2,1)} H^{\tilde{1},1} \left(\frac{\vec{u}^n}{\Delta t} - \text{ conv }^n - \frac{1}{Re} H^{1,1} \tilde{\mathbb{E}}^{(1,0)} H^{\tilde{0},2} \left(\xi^n + \xi_{\text{prescr}}\right)\right) + \frac{\vec{u}_{\text{norm}}}{\Delta t} \tag{2.16}$$

Chapter 3

Computational Set Up

The discretized Navier-Stokes equations discussed in the previous section are representative of a staggered scheme, where variables are defined on either a primal or dual grid. This chapter discusses the construction of physical meshes pertinent to the lid-driven cavity problem, on which the discrete system may be numerically solved. An overview of the numerical solution procedure and its implementation in MATLAB is also provided.

3.1 Primal Mesh

3.1.1 Structure

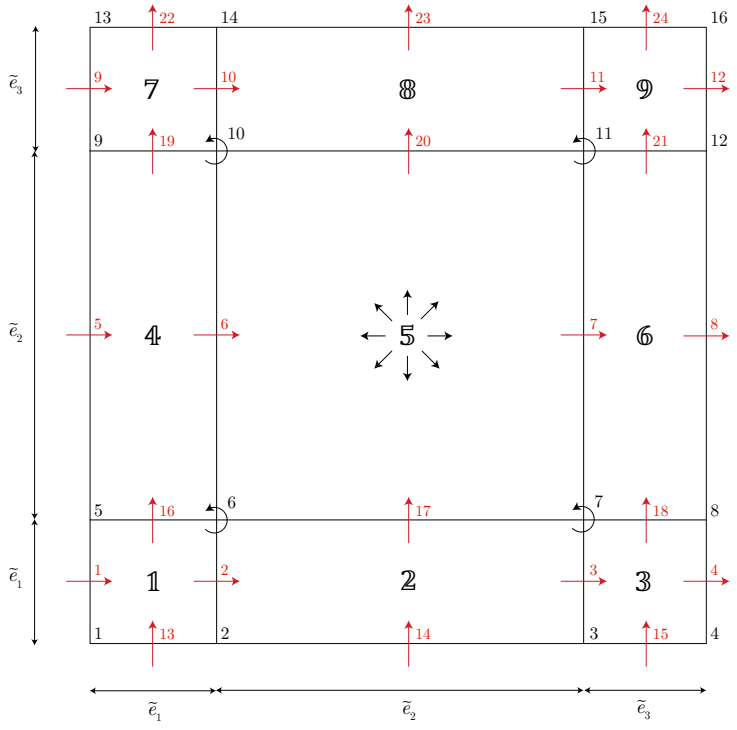

Figure 3.1: Structure and conventions of the primal mesh for $N = 3$.

The variables on the upper-branch of the De-Rham sequence are defined on the primal mesh. The square mesh is structured and orthogonal, and extends from (0,0) in the lower-left corner to (1,1) in the upper-right corner representing the non-dimensionalized bounds of the cavity. The number of inner points on the primal mesh is equal to $(N+1)^2$ and their ordering is selected to be lexicographic along x. The sense of rotation at each of the primal points is defined to be anti-clockwise. Similarly, the $2N(N+1)$ primal edges are also ordered lexicographically with positive flux conventions defined as per Figure 2.1. The primal surfaces are treated as sources and the primal edge lengths are shown as $\tilde{e}$.

3.1.2 Incidence Matrices

$\tilde{\mathbb{E}}^{(2,1)}$

The first operation we consider is the primal divergence $\boldsymbol{\nabla}\cdot$, represented in discrete form by the incidence matrix $\tilde{\mathbb{E}}^{(2,1)}$. This matrix associates variables defined over primal edges to those defined over the primal surfaces. Edges with a convention aligned with the source-like behaviour of surfaces are assigned a value of 1 within the matrix, while those with an opposing convention are assigned -1.

The primal mesh for this problem is appended with additional surfaces along its boundary, where the corresponding fluxes may be prescribed. This is shown in Figure 3.2.

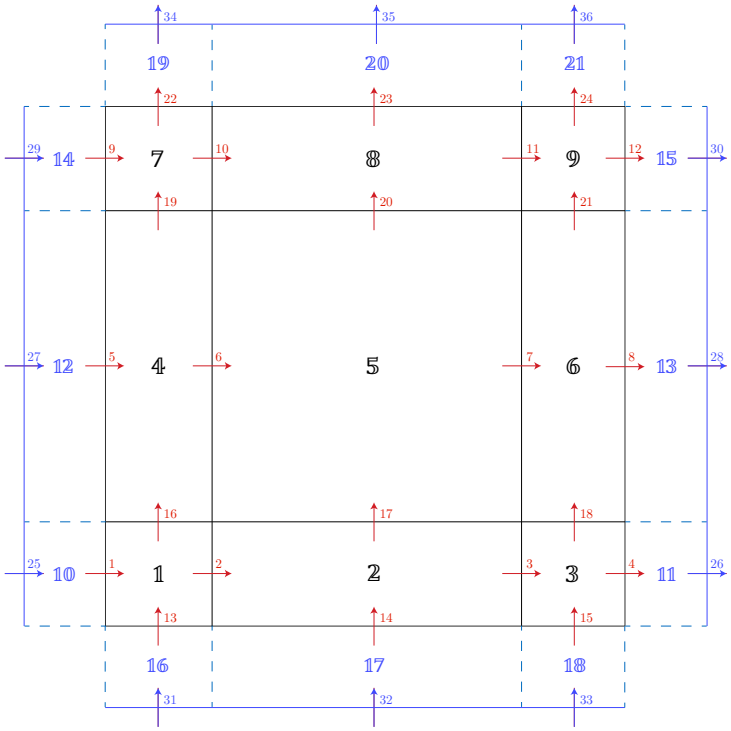

Figure 3.2: The primal mesh with appended boundaries, for $N = 3$.

The ordering of the appended surfaces and edges is such that the structure of the matrix $\tilde{\mathbb{E}}^{(2,1)}$ is divided into four distinct blocks.

$$\tilde{\mathbb{E}}^{(2,1)} = \begin{bmatrix} B_1 & B_2 \\ B_3 & B_4 \end{bmatrix} \tag{3.1}$$

where,

- B_1 relates the inner edges and surfaces
- B_2 relates the boundary edges and inner surfaces
- B_3 relates the inner edges and boundary surfaces
- B_4 relates the boundary edges and surfaces

This allows for the blocks that map prescribed values at the boundary edges to be removed from the $\tilde{\mathbb{E}}^{(2,1)}$ and assembled into a boundary matrix $\mathbb{E}_{\text{norm}}$ such that:

$$\boldsymbol{\nabla} \cdot u = \tilde{\mathbb{E}}^{(2,1)} \tilde{u} + \mathbb{E}_{\text{norm}} \tilde{u}_{\text{boundary}} \tag{3.2}$$

with the quantities defined as,

$$\begin{aligned} \tilde{\mathbb{E}}^{(2,1)} &= \begin{bmatrix} B_1 \\ B_3 \end{bmatrix} \\ \mathbb{E}_{\text{norm}} &= \begin{bmatrix} B_2 \\ B_4 \end{bmatrix} \\ \tilde{u}_{\text{boundary}} &= \int_{\text{boundary}} u \mathrm{d}\tilde{e} \end{aligned} \tag{3.3}$$

The inner($\tilde{\mathbb{E}}^{(2,1)}$) and boundary($\mathbb{E}_{\text{norm}}$) matrices can now be constructed independently as sparse matrices in MATLAB. For the lid-driven cavity problem the vector of known boundary fluxes is zero, as per the no-slip condition.

$\tilde{\mathbb{E}}^{(1,0)}$

The incidence matrix $\tilde{\mathbb{E}}^{(1,0)}$ is a mapping from the primal points to the primal edges and corresponds physically to a curl operation $\boldsymbol{\nabla}\times$ as per the sequence in Figure 2.1. It can be shown that $\tilde{\mathbb{E}}^{(1,0)} = \mathbb{E}^{(2,1)^{\mathrm{T}}}$, whose construction is discussed in the following section.

3.2 Dual Mesh

3.2.1 Structure

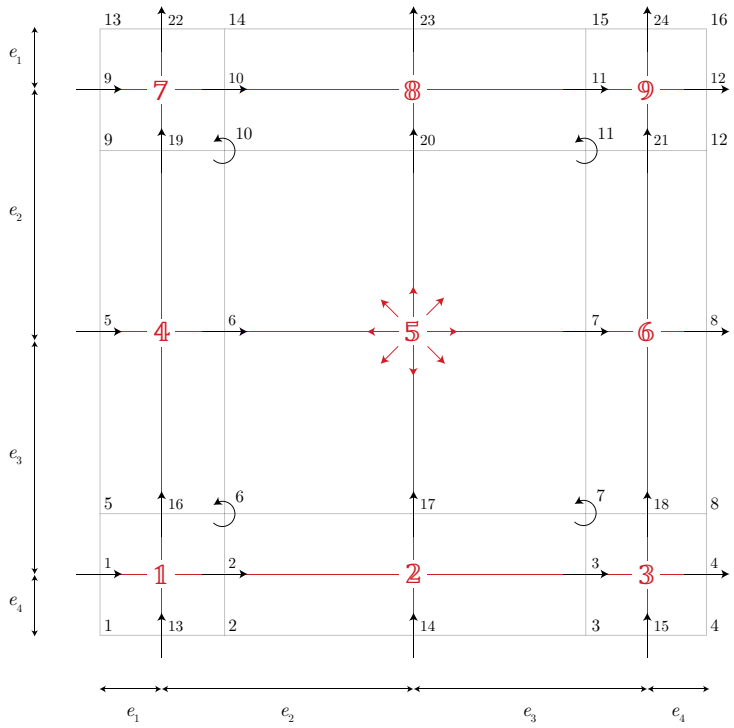

Figure 3.3: Structure and conventions of the dual mesh for $N = 3$.

The variables on the lower branch of the De-Rham sequence are defined on the dual mesh, which is derived from and inherently related to the primal mesh. The dual points correspond to the surfaces of the primal mesh while the dual surfaces are related to the primal points. The dual points are connected by the edges of the dual mesh and all conventions are inherited from the primal mesh. A sample schematic of the dual mesh and its corresponding primal mesh is provided in Figure 3.3

3.2.2 Incidence Matrices

$\mathbb{E}^{(2,1)}$

The operation $\mathbb{E}^{(2,1)}$ associates the surfaces of the dual mesh to its edges, and is representative of the curl operator $\nabla\times$. Similar to $\tilde{\mathbb{E}}^{(2,1)}$, the entries of the incidence matrix are 1 if the dual edges are aligned with the counter-clockwise convention of a dual surface, -1 if they are in opposition and 0 if the surface and edge are unrelated. As the variable defined on the dual edges is a line-integral of the velocity along the edge (equation 2.11), the operation $\mathbb{E}^{(2,1)}u$ is the circulation associated to each dual surface. According to Stoke's law this is equal to the integrated vorticity ξ over the dual surfaces.

As the dual mesh is not a cell complex, extra boundary edges are required to make it so. The no-slip condition for the velocity may then be prescribed along these edges. This is shown in Figure 3.4.

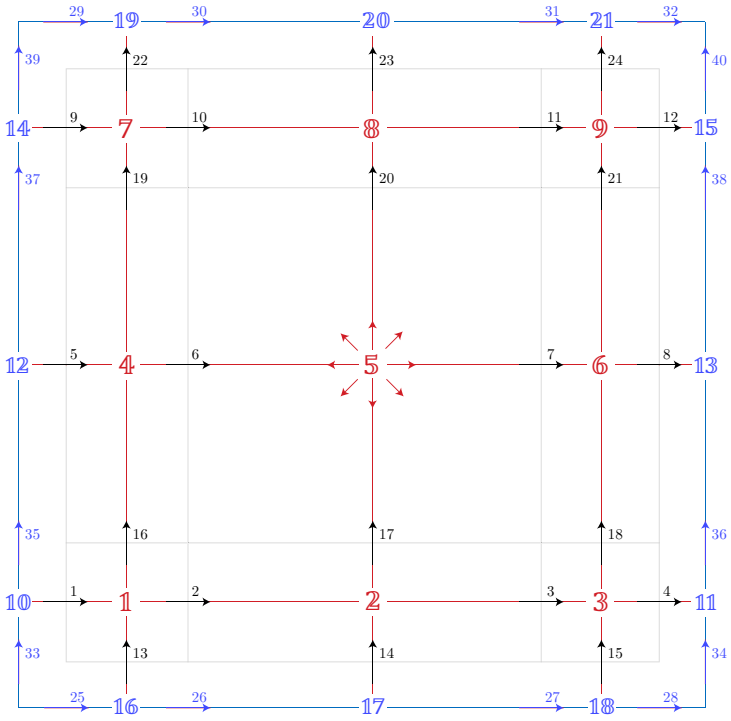

Figure 3.4: The dual mesh with appended boundaries, for $N = 3$.

In a similar manner to that of $\tilde{\mathbb{E}}^{(2,1)}$, the boundary edges are ordered such that the incidence matrix $\mathbb{E}^{(2,1)}$ can also be split into four blocks, allowing for:

$$\boldsymbol{\nabla} \times u = \mathbb{E}^{(2,1)} u + \mathbb{E}_{\tan} u_{\text{boundary}} \tag{3.4}$$

where the inner and boundary matrices are defined analogously to equation 3.3. As the upper boundary of the cavity translates to the left at a unit velocity, the vector of knowns is non-zero as per the no-slip condition. In the context of equation 3.4, this is the contribution of the boundaries to the integrated vorticity in the cavity.

$\mathbb{E}^{(1,0)}$

The operation represented by $\mathbb{E}^{(1,0)}$ can be interpreted as the gradient $\boldsymbol{\nabla}$ of a variable defined on the dual points, mapping them to the dual edges. In a staggered-scheme discretization of the Navier-Stokes equations, this matrix operates exclusively on the vector of pressure unknowns and is constructed as $\mathbb{E}^{(1,0)} = -\tilde{\mathbb{E}}^{(2,1)^{\mathrm{T}}}$.

3.3 Hodge Matrices

The transformation between corresponding quantities on the upper and lower branches of the De Rahm sequence is done through the Hodge matrices, discussed conceptually in section 2.2.2. The Hodge matrices also contain physical information pertinent to the discretization scheme and are inherently square matrices, as they map to an equivalent number of degrees of freedom. The discretization of the Navier-Stokes equations for this cavity-flow problem involves the construction of Hodge matrices for two variables - velocity and vorticity.

3.3.1 Velocity

As discussed in section 2.2.2, the assumption of a constant velocity over a dual/primal edge is made in order to relate the velocity-related degrees of freedom defined on each mesh. This allows for equation 2.13 to be derived, where the ratio of edge lengths is used to convert between the fluxes on the primal mesh, and circulations on the dual mesh. The square Hodge matrix $\mathbb{H}^{(\tilde{1},1)}$ is then constructed as a sparse diagonal matrix in MATLAB, such that:

$$\tilde{u} = \mathbb{H}^{(\tilde{1},1)} u \tag{3.5}$$

The reverse operation, which transforms the fluxes on the primal mesh into their corresponding circulations on the dual mesh, requires the inverse of $\mathbb{H}^{(\tilde{1},1)}$. As the matrix is square and diagonal, $\mathbb{H}^{(1,\tilde{1})}$ is constructed using the reciprocal of the diagonal in $\mathbb{H}^{(\tilde{1},1)}$.

$$u = \mathbb{H}^{(\tilde{1},1)^{-1}} \tilde{u} = \mathbb{H}^{(1,\tilde{1})} \tilde{u} \tag{3.6}$$

3.3.2 Vorticity

A Hodge matrix is required to convert the integrated dual vorticity ξ into a vorticity defined over the primal points $\tilde{\xi}$, as part of the discretization of the viscous terms in the Navier-Stokes equations. Similar to the velocity, the assumption that the vorticity is constant over a dual surface is made. This allows for the following relation to be derived:

$$\frac{\tilde{\xi}}{\xi} = \frac{\vec{\boldsymbol{\xi}}}{\iint_S \vec{\boldsymbol{\xi}} \cdot \mathrm{d}s} = \frac{1}{S} \tag{3.7}$$

Where S is the area of a dual surface. The Hodge matrix can once again be constructed as a square, diagonal matrix where the diagonal is the reciprocal of the dual surface area vector.

$$\tilde{\xi} = \mathbb{H}^{(\tilde{0},2)} \xi \tag{3.8}$$

3.4 Solution Procedure

3.4.1 Convective Term

The convective term is the source of non-linearity in the Navier-Stokes equations and leads to a challenging solution procedure in most CFD applications. We can expand the expression $-\vec{u} \times \vec{\xi}$ in equation 2.8 as:

$$-\vec{u} \times \vec{\xi} = \begin{vmatrix} \hat{\mathbf{i}} & \hat{\mathbf{j}} & \hat{\mathbf{k}} \\ u_c & v_c & 0 \\ 0 & 0 & \xi_c \end{vmatrix} = -v_c \xi_c \hat{\mathbf{i}} + u_c \xi_c \hat{\mathbf{j}} \tag{3.9}$$

The quantity ξ_c is equal to the vorticity at the primal points $\tilde{\xi}$, while u_c and v_c are approximations of velocity at the primal points. The circulations assigned to the dual edges are converted into their respective velocities (through equation 2.12) and averaged around each corresponding primal point. This allows for the products in equations 3.9 to be evaluated on the primal mesh and then interpolated back into the dual edges for use in the discrete momentum equation. For the forward Euler time stepping scheme (section 3.4.3) used in this lid-driven cavity solver the degrees of freedom used to evaluate the convective term at each time step are known, obtained from the solution at the previous time step.

3.4.2 Pressure Singularity

As previously discussed in section 2.3, the total pressure at each time step is determined through the solution of the Poisson equation. The matrix that operates on the total pressure is the discrete form of the Laplacian, obtained as the divergence of the pressure gradient.

$$A = \tilde{\mathbb{E}}^{(2,1)} \mathbb{H}^{(\tilde{1},1)} \mathbb{E}^{(1,0)} = \boldsymbol{\nabla} \cdot \boldsymbol{\nabla} = \nabla^2 \tag{3.10}$$

The zero-flux boundary conditions prescribed at the walls of the cavity correspond to the pressure gradient across the boundaries being zero as well. This is representative of a Neumann-type boundary condition applied to the total pressure and implies that the solution is unique only up to an additive constant. This can be further seen in the singular nature of the Laplacian pressure matrix A.

A deeper insight into the behaviour of the singular system can be obtained through an eigenvalue decomposition of the Laplacian matrix i.e. $A = V \Lambda V^{-1}$, where Λ is a diagonal matrix of the eigenvalues of A and V is a matrix whose columns consist of the corresponding eigenvectors. As A is real and symmetric, the set of eigenvectors is orthonormal and $V^{-1} = V^T$. The eigenvalues and eigenvectors of A are computed numerically using MATLAB, with the existence of a zero is eigenvalue expected from the

singular nature of A. The normalized eigenvector corresponding to the zero eigenvalue is a constant i.e. a contour plot of this eigenvector shows a constant distribution of magnitude $1/\sqrt{N}$. From the definition of an eigenvalue-eigenvector pair ($A\mathbf{v} = \lambda\mathbf{v}$), we see that for the zero eigenvector $A\mathbf{v}_0 = 0$. This implies that A maps a vector whose elements are constant to zero, allowing for an arbitrary constant to be added to the total pressure without affecting the operation $A\mathbf{P}$.

MATLAB determines an arbitrary magnitude for the total pressure solution but preserves its shape, as the gradients are determined from a velocity field satisfying the Navier-Stokes equations. In order to maintain comparability with Botella & Peyret, a constant is subtracted from this total pressure solution such that the static pressure is zero at the centre of the cavity.

3.4.3 Time Stepping

The time derivative is discretized using the forward Euler marching scheme, as shown in section 2.3, and allows for a relatively easier numerical solution procedure. However, the scheme is sensitive to the choice of time step size, and exhibits mathematical instability for large time steps. An initial estimate of the time step size is obtained from the following:

$$\Delta t = \min\left(h_{\min}, \frac{1}{2}\mathrm{Re}\ h_{\min}^2\right) \tag{3.11}$$

Stability tests using this estimate show that the scheme remains stable for a time step as large as five times that computed using the above equation. Thus, this multiplicative factor of 5 is used to increase the time step size and reduce computational time.

Additionally, a metric is required in order to quantify the onset of a steady state for termination of the solution procedure. This is done through an estimation of the time derivative $\partial u/\partial t$. For a stationary process, $\partial u/\partial t$ is ideally zero and the solution is time-invariant. However, in a numerical framework this can be represented by the discrete form of $\partial u/\partial t$ falling below a prescribed tolerance. For the current cavity-flow problem, the convergence criterion $\Delta u/\Delta t < 10^{-5}$ was determined to be an appropriate indication of steady state. A tolerance higher than this poses a risk of the solver terminating the time-stepping sequence without fully achieving a steady state, while lower tolerances ($< 10^{-5}$) unnecessarily led to an increase in computational time. The selected tolerance level was maintained for all computations to ensure consistency, and compatibility of solutions for varying N.

3.4.4 Code Algorithm

The code is initialised with user input for the number of elements N, the Reynolds number Re, and the convergence tolerance. The algorithm then progresses such that it creates the primal and dual mesh based on the prescribed N and the dimensions of the cavity, which are non-dimensionalized to be unity. A series of functions are then called which generate the required incidence, Hodge and boundary matrices, constructed as discussed in sections 3.1, 3.2 and 3.3. The zero initial conditions for the pressure and velocity are then assigned and a suitable time step is determined by the solver. The time-stepping sequence is then entered and the governing equations are solved as follows: The vorticity is computed from the velocity-vorticity relation, along with the convective and diffusive components of the momentum equations. The previously derived pressure Poisson equation is then solved for an updated total pressure. This is then re-inserted into the momentum equation to compute the corresponding updated velocity vector. After this sequence of operations, the discrete time derivative $\partial u/\partial t$ is computed and compared with the selected tolerance to determine whether the solution has effectively reached steady state. If not, the solver advances to the next time step and uses the updated velocity field to repeat the solution procedure for the new time. Additionally, monitors are set-up to verify that the updated velocity field is indeed divergence free. Once the solution has converged to a steady state, additional variables such as the stream function and static pressure are computed. The code is terminated after writing the obtained results to a file for further post-processing.

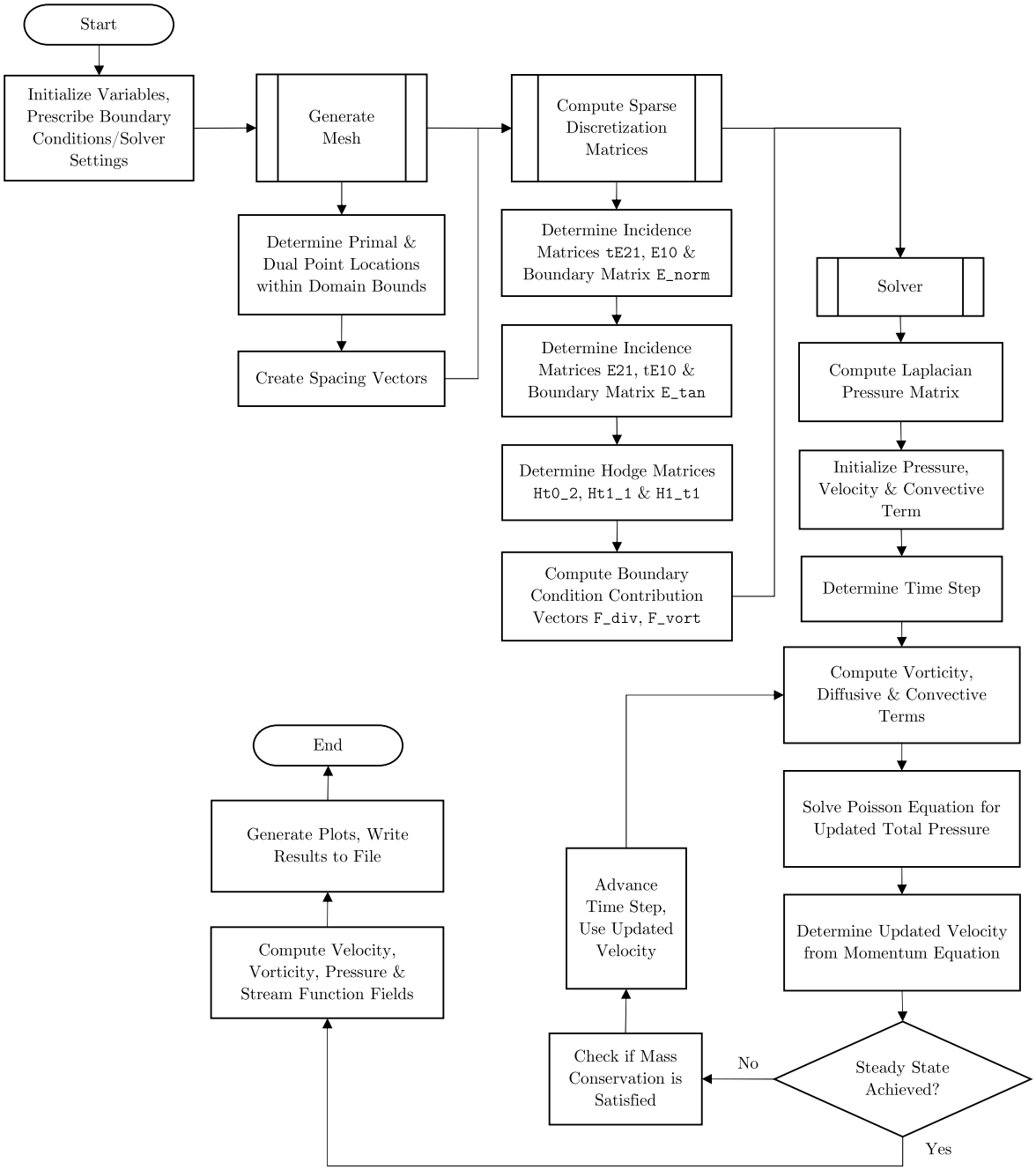

Figure 3.5: Flow chart detailing the progression of the solver algorithm.

Chapter 4

Results of Simulations

In this section of the report, we present the results of the simulations. Comparisons are made to the test case presented by Botella and Peyret. In particular we compare the pressure field, vorticity field, and the stream function for the values N = 15,31,47,55,63. We also plot the pressure, vorticity , x- and y- components of the velocity along the lines $x, y = 0.5$ for the above mentioned values of N. These comparisons are made to the reference values of Botella and Peyret (Botella & Peyret,).

4.1 Contour Plots

4.1.1 Vorticity

We take a look at the contours for the vorticity field. As a requirement, the isolines have been kept consistent with the ones defined in Botella and Peyret. As expected a crude mesh leads to poor spatial resolution and does not effectively capture the isolines and thus the vorticity. As the mesh is made finer the spatial resolution increases and we the vorticity is better captured. This closely resembles the vorticity contour presented in the test case. The test case has a higher spatial resolution thus some differences can be expected. The white parts of the plot highlight the points where the vorticity is too high. In general, we see that vorticity is high along the top boundary as it swirls around the central vortex.

The integrated vorticity in the domain can be determined through through a summation of ξ over the dual surfaces and has a value of unity for all N and Re, thus independent of the discretization. This can be explained through the boundary conditions pertinent to the lid-driven cavity. The initial velocity within the cavity is zero while the lid moves at a unit velocity to the left, creating a discontinuity at the boundary. The magnitude of vorticity (a derivative of the velocity) is thus infinite and resembles the delta-peak function. However, the integrated vorticity is finite and the non-dimensionalization of the problem makes its value unity. As the flow evolves in time, vorticity is diffused throughout the cavity but remains conserved, resulting in a constant integrated vorticity.

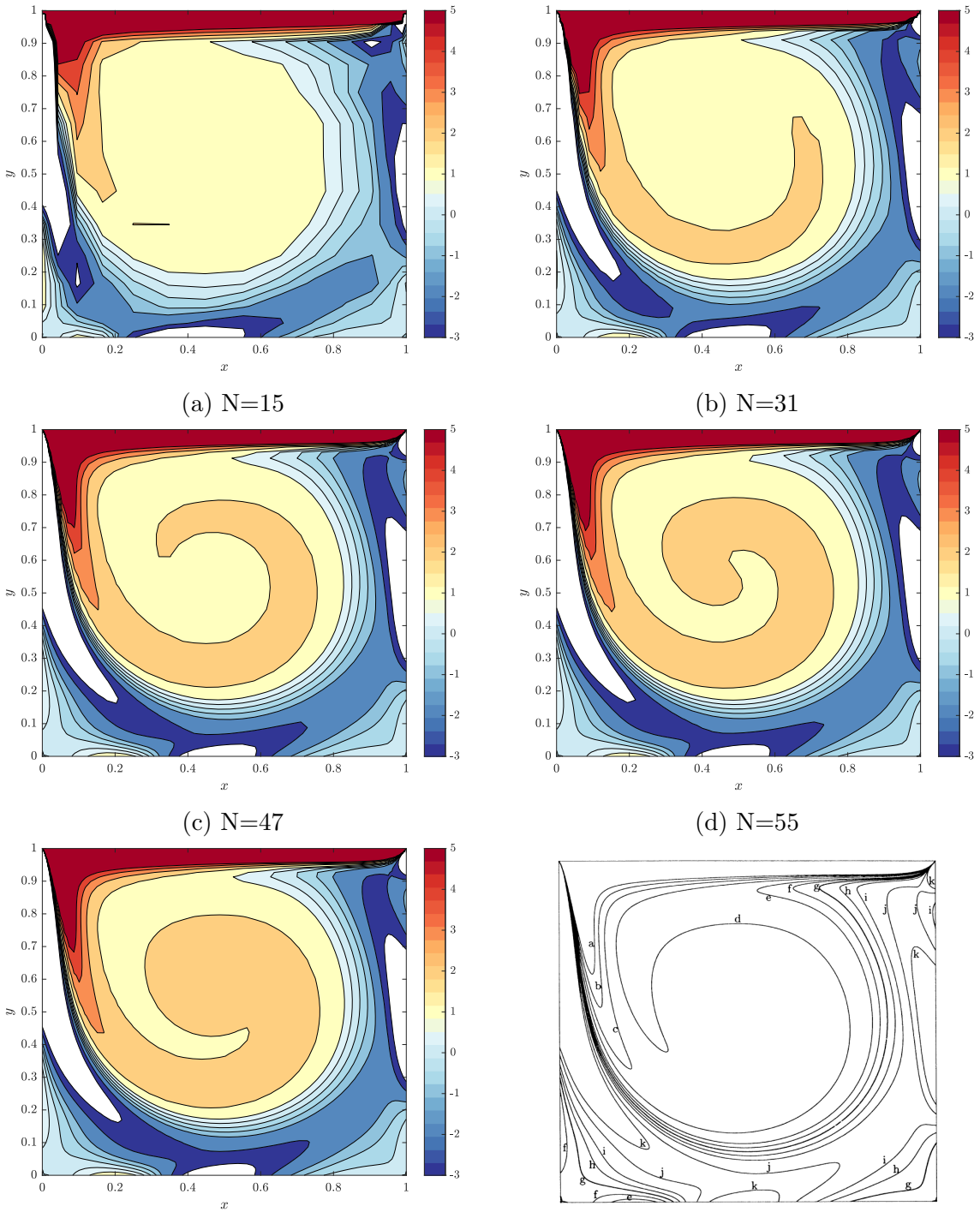

(a) N=15 (b) N=31

(c) N=47 (d) N=55

(e) N=63 (f) N=128 (Botella & Peyret)

Figure 4.1: Contours of vorticity for varying N, at levels defined by (Botella & Peyret,).

4.1.2 Stream Function

The stream function ψ can be evaluated through solving a Poisson equation for it, using the vorticity ξ.

$$\nabla^2\psi = -\xi \implies \boldsymbol{\nabla} \times \boldsymbol{\nabla} \times \psi = \xi \tag{4.1}$$

In discrete from, this equation becomes:

$$\mathbb{H}^{(\tilde{0},2)}\mathbb{E}^{(2,1)}\mathbb{H}^{(1,\tilde{1})}\tilde{\mathbb{E}}^{(1,0)}\psi = \mathbb{H}^{(\tilde{0},2)}\mathbb{E}^{(2,1)}u \tag{4.2}$$

We take a look at the contours for the stream function in this section. As a requirement, the isolines have been kept consistent with the ones defined in Botella and Peyret. With lower discretization, the streamlines are not smooth. They are coarse and do not convey information accurately. As we increase the discretization, the spatial resolution increases and we see the isolines becoming smoother. Compared to the least discretized case, we see that more streamlines are being defined. The isolines are consistent with the presence of the central vortex as seen in the previous section. The highest value of the stream function is seen at the center of the domain and the values decrease outwards. This result is reinforced by the pressure contours. Secondary vortices are seen in the bottom corners. The white patches reveal areas where the value of the stream function are too high.

4.1.3 Pressure

We take a look at the pressure contours in this section. As a requirement, the isolines have been kept consistent with the ones defined in Botella and Peyret. The lower discretization poorly captures the pressure fields. The isolines are not smooth and there are significant errors in the predicted field. This changes with increasing discretization. We see that the pressure is low in the center of the domain. This corresponds well with the other contour plot as this low pressure region in the center correlates with the vorticity as well as the stream function. Some regions in the pressure field are white as they represent extreme pressure values.

4.2 Centreline Plots

4.2.1 Velocity

In this section we look at the centerline plots of the u- and v- component of the velocity along the vertical and horizontal centerlines. Let us consider Figure 4.4, which deals with the u-velocity component. Figure a shows the horizontal centerline while the Figure b shows the vertical center line. We see that in the horizontal centerline the the boundary conditions are respected and there is zero velocity on the boundaries. In the case of the vertical centerline, the top wall has a non-zero boundary condition. This is reflected in the plot as the value of the u-component is -1 at the top wall. As is expected, the plots get closer to one another as the spatial resolution increases. The low discretization values remain to be outliers.

In the Figure 4.5, we look closely at the v-component of the velocity. Figure a shows the horizontal centerline while the Figure b shows the vertical center line. In both the

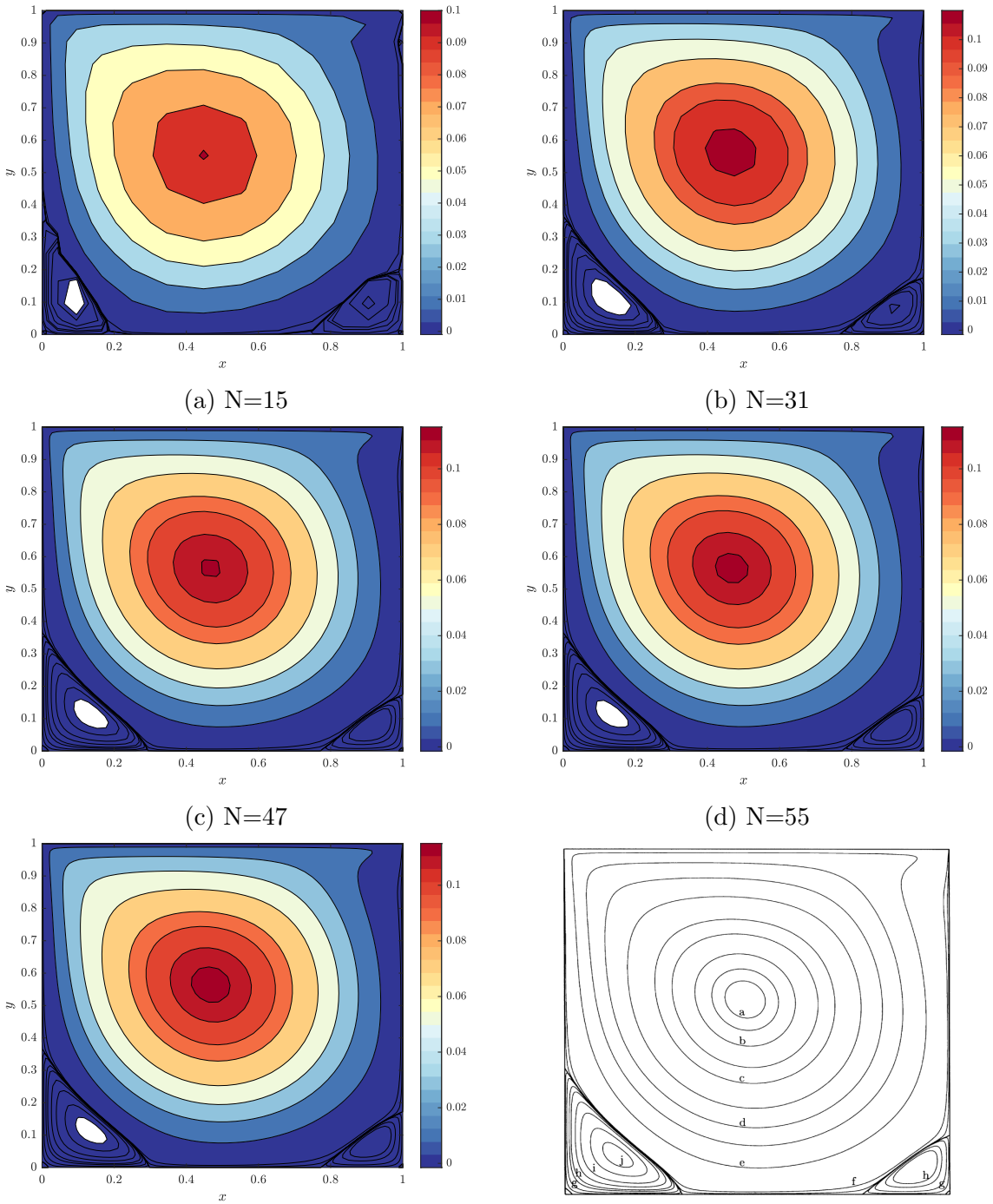

(a) N=15

(b) N=31

(c) N=47

(d) N=55

(e) N=63

(f) N=128 (Botella & Peyret)

Figure 4.2: Contours of stream function for varying N, at levels defined by (Botella & Peyret,).

cases of the centerline, we see that the velocity is zero at the boundaries, while it remains non-zero inside the domain. Increasing the spatial resolution brings the velocity values closer to the reference values.

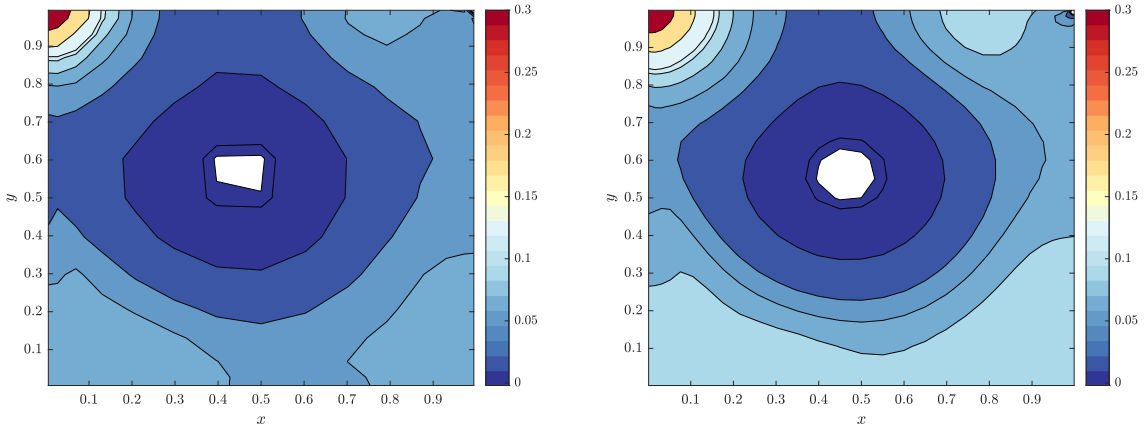

(a) N=15

(b) N=31

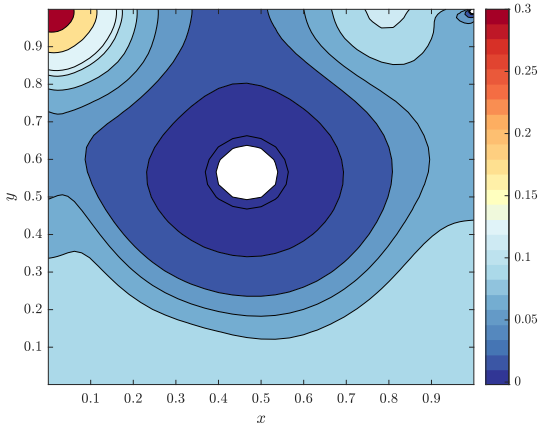

(c) N=47

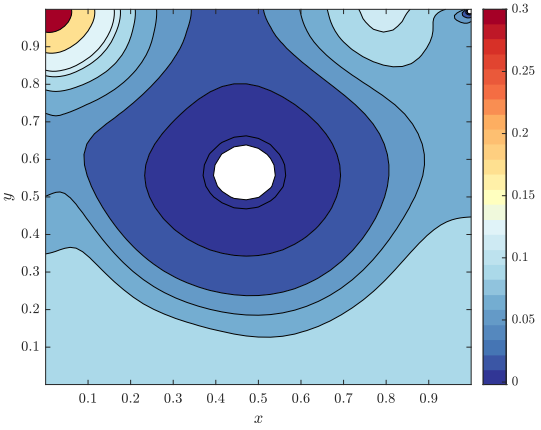

(d) N=55

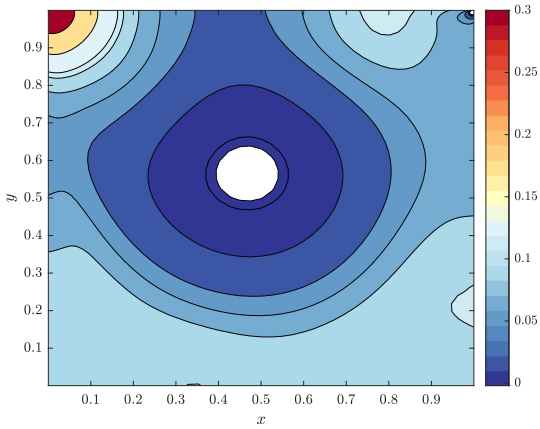

(e) N=63

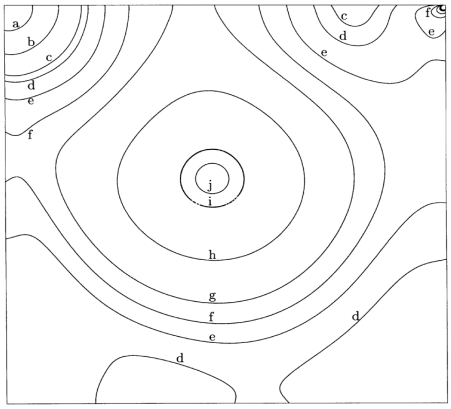

(f) N=128 (Botella & Peyret)

Figure 4.3: Contours of pressure for varying N, at levels defined by (Botella & Peyret,).

4.2.2 Pressure

In this section we look at the variation of the pressure along the vertical and horizontal centerlines. Figure 4.6 a shows the horizontal centerline while Figure 4.6 b shows the variations along the vertical center line. In both cases, we see the pressure variations that corroborate the pressure contours. We see that in the middle of the domain, there pressure reaches it's lowest values, while increasing towards the boundaries. The lower

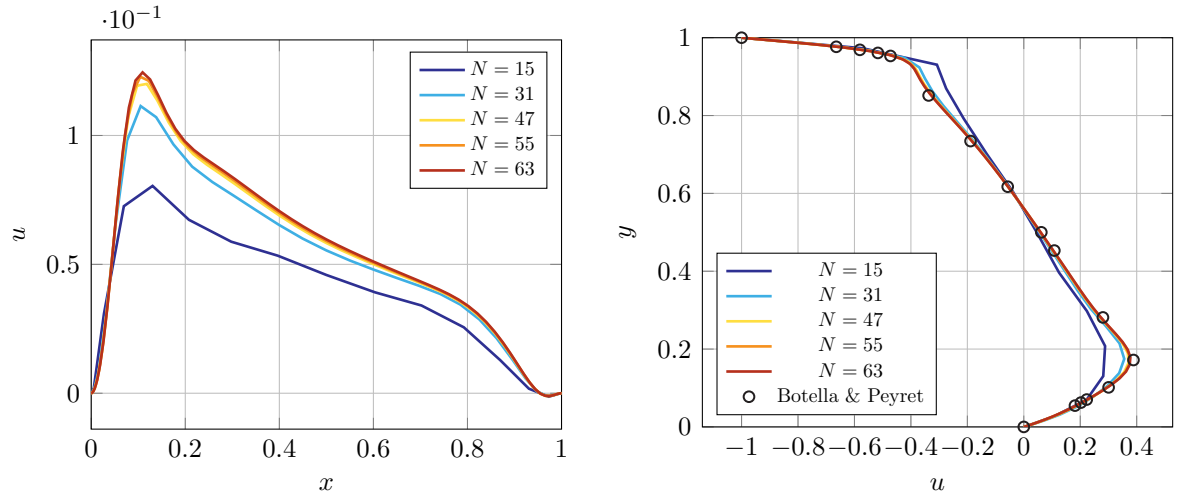

(a) $y = 0.5$ (b) $x = 0.5$

Figure 4.4: Variation of $u-$velocity along the horizontal and vertical cavity centrelines.

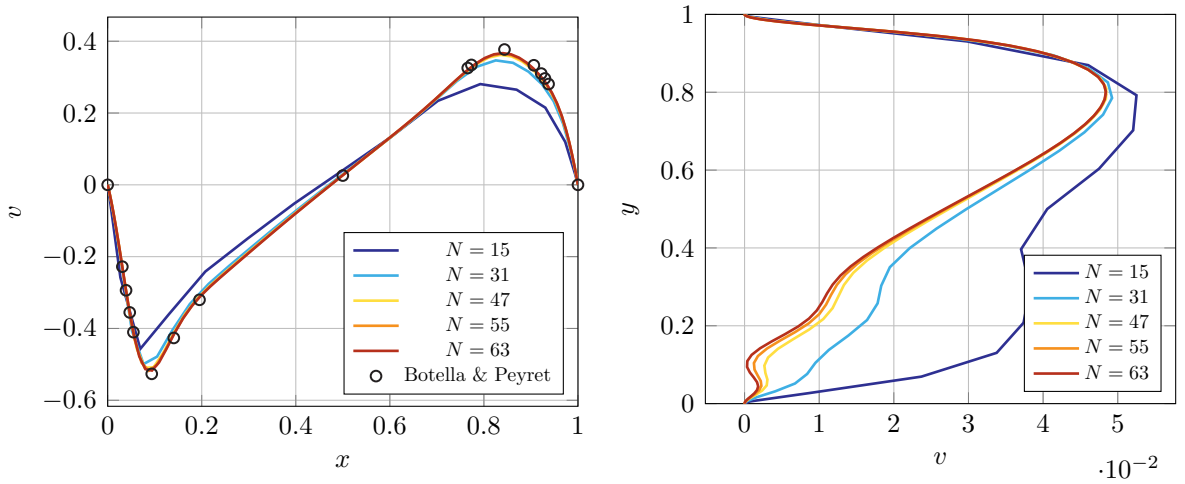

(a) $y = 0.5$ (b) $x = 0.5$

Figure 4.5: Variation of $v-$velocity along the horizontal and vertical cavity centrelines.

spatial resolution leads to erroneous results, while increasing it causes the pressure to converge to the reference value.

4.2.3 Vorticity

Last but not the least, we look at the variations of the vorticity along the horizontal and vertical centerlines. Figure 4.7 a shows the variations along the horizontal centerline while the Figure 4.7 b shows the variations along the vertical centerline.

Along the horizontal centerline, we see that there is significant negative vorticity. This negative vorticity is concetrated at the edges of the domain. These vorticity values can be corroborated from the vorticity contours discussed above. The maximum vorticity is seen at $x \approx 0.15, 0.2$.

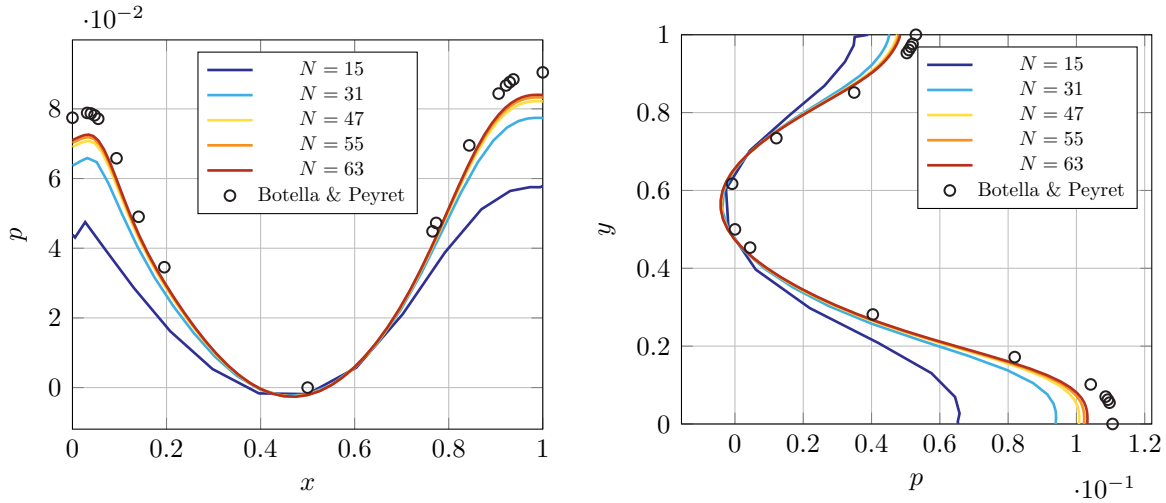

(a) $y = 0.5$ (b) $x = 0.5$

Figure 4.6: Variation of pressure along the horizontal and vertical cavity centrelines.

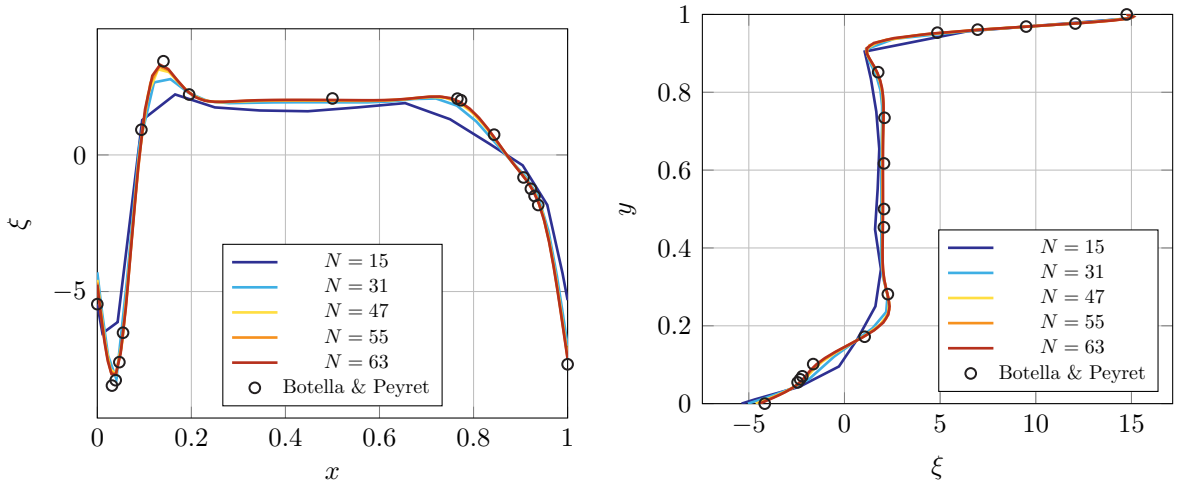

(a) $y = 0.5$ (b) $x = 0.5$

Figure 4.7: Variation of vorticity along the horizontal and vertical cavity centrelines.

Looking at the vertical centreline, we see that the negative vorticity is limited to the bottom of the domain. While at the top of the domain we see a region of high vorticity that is induced from the boundary conditions.

Chapter 5

Conclusions

A Navier-Stokes solver was developed to solve the lid-driven cavity problem for two-dimensional flow. This was done by utilizing incidence and Hodge matrices to transfer information from the primal to the dual mesh. The aforementioned vector operations are implemented by referring to the double De Rahm. The equations were solved on a N $\times$ N discretized grid. In specific, the investigations were preformed for N = 15,31,47,55, and 63. The report also details the various concepts of the dual and primal mesh that are utilised while building the numerical mode.

The results of the simulation were validated against the results obtained by Botella and Peyret (Botella & Peyret,) who performed their simulations at N = 128. In general, it was found that for dense grids, the results closely matched to those obtained by Botella and Peyret. On the other hand, a coarse grid presented results with large errors, which ideally are resolved by making the grid finer. Contour plots were developed for vorticity and the stream function, while centerline plots were plotted for the variations in velocity, pressure, and voriticity.

Better results can be obtained by performing a grid convergence study, that aims at finding an optimal grid discretization beyond which the results are not greatly varied, in the interest of computational efficiency. The processing can be made better by using more powerful computers and using concepts such as parallel computing, etc.

References

Botella, O., Peyret, R. (1998). Benchmark spectral results on the lid-driven cavity flow. *Computers & Fluids*, *27*(4), 421–433.